

Review

Prospective of (BaCa)(ZrTi)O₃ Lead-free Piezoelectric Ceramics

Wenfeng Liu *, Lu Cheng and Shengtao Li

State Key Laboratory of Electrical Insulation and Power Equipment, Xi'an Jiaotong University, Xi'an 710049, China; lu.cheng@stu.xjtu.edu.cn (L.C.); sli@xjtu.edu.cn (S.L.)

* Correspondence: liuwenfeng@xjtu.edu.cn

Received: 11 February 2019; Accepted: 13 March 2019; Published: 26 March 2019



Abstract: Piezoelectric ceramics is a functional material that can convert mechanical energy into electrical energy and vice versa. It can find wide applications ranging from our daily life to high-end techniques and dominates a billion-dollar market. For half a century, the working horse of the field has been the polycrystalline PbZr_{1-x}Ti_xO₃ (PZT), which is now globally resisted for containing the toxic element lead. In 2009, our group discovered a non-Pb piezoelectric material, (BaCa)(ZrTi)O₃ ceramics (BZT-BCT), which exhibits an ultrahigh piezoelectric coefficient d_{33} of 560–620 pC/N. This result brought extensive interest in the research field and important consequences for the piezoelectric industry that has relied on PZT. In the present paper, we review the recent progress, both experimental and theoretical, in the BZT-BCT ceramics.

Keywords: piezoelectric; ceramic; lead-free

1. Introduction

Piezoelectricity refers to the phenomenon of interconversion between mechanical energy and electrical energy, which yields a mechanical-stress-induced polarization or an electrical-field-induced strain. Such ability of energy conversion enables piezoelectric materials to be widely used in devices such as sensors, actuators, transducers, etc. [1,2]. For more than half a century, Pb-based piezoelectric ceramics (e.g. PbZr_{1-x}Ti_xO₃, PbMg_xNb_{1-x}-PbTiO₃ and PbZn_xNb_{1-x}-PbTiO₃) have dominated the area of most applications. However, the use of Pb-based materials is restricted by increasingly tight regulations due to its high toxicity [3,4]. This arouses extensive investigations on the mechanism of high piezoelectricity in Pb-based materials and the exploration of Pb substitutes [5–8].

In 2009, a large piezoelectric performance with d_{33} of 620 pC/N was observed for 0.5Ba(Zr_{0.2}Ti_{0.8})O₃-0.5(Ba_{0.7}Ca_{0.3})TiO₃ composites (BZT-50BCT) [9]. Later, the modified BZT-BCT composite ceramics showed a higher $T_c \sim 114$ °C than BZT-0.53BCT [10]. By optimizing the poling conditions, BZT-BCT ceramics combines a large piezoelectric performance with d_{33} of 630 pC/N and the planar electromechanical factor of 56% [11]. Yang et al. prepared the lead-free BZT-BCT ceramics by sol-gel technique [12], whose maximum permittivity was above 9000 with a maximum converse piezoelectric coefficient (d_{33}^*) of 400 pm/V.

In this review, we summarize the recent progresses on BZT-BCT piezoelectric ceramics by different doping mechanisms that may offer some thoughts on the future improvement of BZT-BCT and even other piezoelectric ceramics. Further, the potential application of BZT-BCT ceramics are presented, including electrocaloric effect, fluorescence and energy storage. Based on the current achievements, we also propose some prospects, which may provide new directions on the development of BZT-BCT ceramics.

2. MPB Strategy

In both Pb-based and Pb-free piezoelectric systems, the common solution to promote piezoelectric performance is to place materials at their phase transition boundaries, either a paraelectric to ferroelectric phase boundary or multi ferroelectric phases coexisting boundary (including the most famous morphotropic phase boundary, i.e. MPB), since the instability of the polarization at phase boundaries allows a significant polarization variation under an external stress or electric field. Despite the intense interests in the phase coexisting strategy, the key to understanding the consequent high piezoelectricity in BZT-*x*BCT ceramics is still in dispute. For instance, we initially proposed the coexistence of tetragonal (T) and rhombohedral (R) symmetry at MPB, evidenced by the synchrotron X-ray diffraction (XRD) results from Ehmke [13] and transmission electron microscope (TEM) results from Gao [14]; however, soon after, the discovery of an intermediate orthorhombic (O) phase was found based on synchrotron XRD results from Keeble [15,16] and temperature spectrum of dielectric permittivity from Damjanovic [17].

In addition, the phenomenological Landau–Devonshire model suggests that the reduction of polarization anisotropy is responsible for enhanced piezoelectric response approaching to MPB [18,19]. Acosta calculated the anisotropy energy of a sixth-order Landau potential formulated for the BZT-*x*BCT system and found that the anisotropy energy approaches zero near the O-R rather than the T-O phase boundary. They thus attributed the best piezoelectric property found at the T-O phase boundary to two other factors, i.e., higher degree of poling and increased elastic softening [20]. Ke used the energy barrier along the minimum energy pathway on the free energy surface for direct domain switching to quantitatively measure the degree of polarization anisotropy and suggested that the polarization anisotropy at the T-O phase boundary was the smallest [21].

In most MPB systems (e.g., PMN-PT and PZN-PT), MPB is temperature dependent, similar to the BZT-BCT system, but this does not render such systems useless. Many important applications of this system have been found. The widely used solution to achieve temperature stability is to choose a composition slightly away from the MPB, so that the properties are no longer sensitive over the ambient temperature range. However, this is at the expenses of a slight reduction of piezoelectric properties. It is the same situation in the BZT-BCT ceramics. As shown in Figure 1, by choosing BZT-45BCT, a composition slightly off MPB composition (50BCT), d_{33} becomes almost temperature independent in the room temperature range (20–40 °C). This temperature stability is achieved with some sacrifices of d_{33} , but the d_{33} (~360 pC/N) is still much higher than many other non-Pb piezoelectric materials.

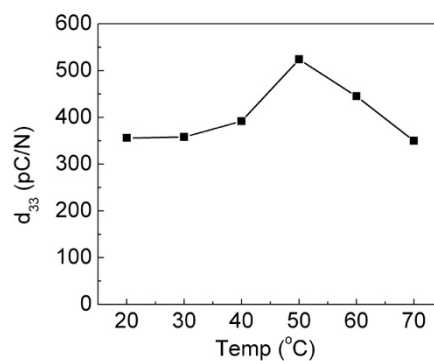


Figure 1. Temperature dependence of d_{33} of BZT-45BCT.

3. Approach to Tailor the Piezoelectric Performance of BZT-BCT

The chemical modification is the most efficient and widely accepted way to tailor the piezoelectric performance of piezoceramics. Table 1 summarizes the most attractive achievements of both pure BZT-BCT ceramic and doped ceramics. Based on the mechanism of chemical modification, the composition optimization can be categorized into improving microstructure by sintering aids and

substitution doping, and the most improved piezoelectric performances of each doping element can be found in Figure 2.

Table 1. Piezoelectric performance of the BZT-BCT based ceramics.

Compositions	d_{33} (pC/N)	k_p	ϵ_r	T_c (°C)	Reference
BZT-50BCT	650	53%	4500	85	[22]
	630	56%		90	[11]
	620		3060	93	[23]
	572	57%	4821	94.8	[24]
	546	65%	4050		[25]
	464		2938		[26]
BZT-50BCT-0.08 wt% ZnO	603				[27]
BZT-50BCT-0.04 wt% CeO ₂	600	51%	4843		[28]
BZT-50BCT-0.1 wt% CeO ₂	565	52%	3860		[29]
BZT-50BCT-0.2 wt% Sr(Cu _{1/3} Ta _{2/3})O ₃	577	#####		97	[30]
99.2 mol% (BZT-50BCT)-0.8 mol% BiAlO ₃	568	54%	3375	72	[31]
BZT-50BCT-0.06 wt% Y ₂ O ₃	560	53%		95	[32]
BZT-50BCT-0.1% Sb ₂ O ₃	556	52%	3985		[33]
(Ba _{0.82} Sr _{0.03} Ca _{0.15})(Zr _{0.1} Ti _{0.9})O ₃	534	#####		84	[34]
BZT-50BCT-0.06 mol% ZnO	521	#####			[35]
BZT-50BCT-1 mol% Sn-1 mol% Sr	514	#####			[36]
BZT-50BCT-0.3 wt% Li ₂ CO ₃	512	49%	4394	79.6	[37]
BZT-50BCT-0.04 wt% CuO	510	45%	3762	95	[38]
BZT-50BCT-0.5 mol% SiO ₂	500				[39]

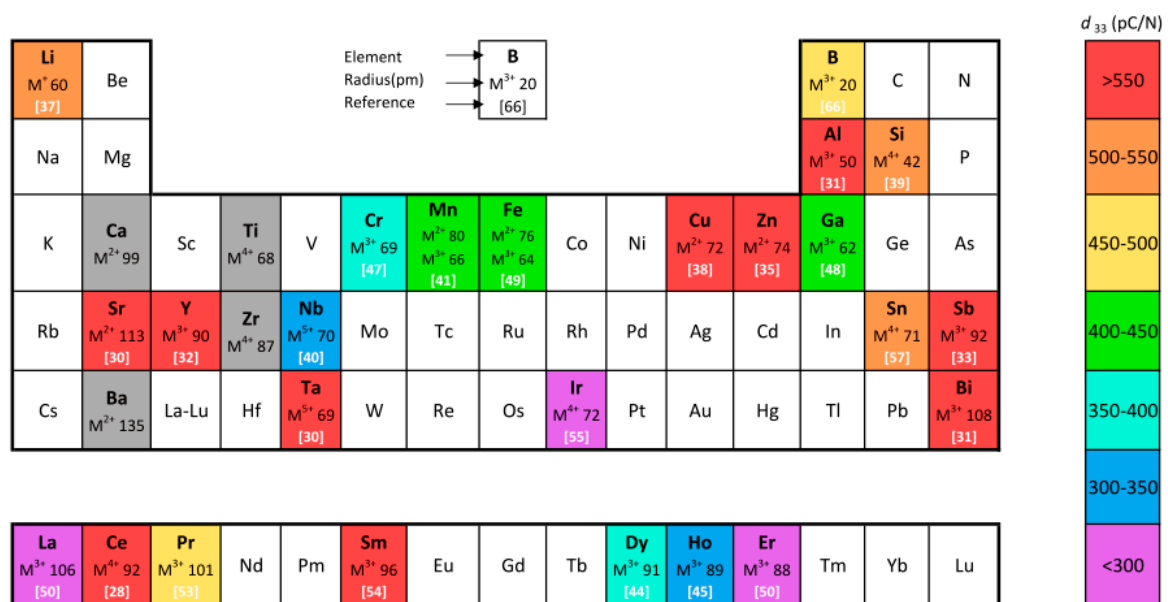


Figure 2. Piezoelectric coefficient (d_{33}) of the point-defects modified BZT-BCT ceramics.

3.1. Substitution Doping

Ferroelectrics are rarely used in a chemically pure form and doping is always employed with the goal of tailoring the properties for specific applications. Different doping usually brings about different consequence, such as acceptor doping to obtain low dielectric losses and donor doping to achieve high piezoelectric coefficients. For the equivalent doping, it is usually employed to modify

the Curie temperature and introduce the compositional disorder, which may also greatly affect the piezoelectric performance. As shown in Figure 2, the radius of Ba^{2+} and Ca^{2+} are 135 pm and 99 pm, respectively, while Ti^{4+} and Zr^{4+} are 68 pm and 87 pm, respectively. Usually, large ions will occupy the A-site, and small ions will occupy the B-site, and intermediate ions will occupy both sites with different ratios of the perovskite structure.

3.1.1. Acceptor Doping

An acceptor dopant has a lower oxidation number than that of the host cation. This will create oxygen vacancies owing to the charge compensation, and the oxygen vacancies can contribute to the mass transport and improve the density during sintering process [27,35,40].

Zn^{2+} has a radius of 74 pm and prefers to replace smaller ions in B-site. JG Wu pointed out that the Zn^{2+} substitution into the $(\text{Ti}, \text{Zr})^{4+}$ site results in both structure disorder and lattice distortion. The presence of oxygen vacancies helps the mass transport during sintering, which is responsible for the enhanced grain growth as the ZnO content increases. Besides, the tricritical point of these ceramics was shifted to room temperature while the Curie temperature decreased simultaneously by the introduction of ZnO. Macroscopically, the BZT-BCT ceramics have $\epsilon_r \sim 4500$ and $\tan\delta < 1.5\%$. BZT-BCT ceramic with 0.06 mol.% ZnO demonstrates an enhanced electrical behavior with $d_{33} \sim 521$ pC/N, $k_p \sim 47.8\%$, and $2P_r \sim 19.37 \mu\text{C}/\text{cm}^2$, owing to the room-temperature tricritical point induced by doping with ZnO [35]. Similar results were also reported by Zhao [27]. In Zhao's work, the BZT-BCT ceramics with 0.08 wt% ZnO show maximum remnant polarization and spontaneous polarization ($P_r = 10.14 \mu\text{C}/\text{cm}^2$, $P_s = 19.68 \mu\text{C}/\text{cm}^2$). At the same time, the giant piezoelectric coefficient of $d_{33} = 603$ pC/N and high planar electromechanical coupling factor of $k_p = 0.56$ were also obtained for the samples. Besides, they revealed that further raising ZnO content would cause partial Zn^{2+} ions occupying A-site, resulting in decrease in lattice parameters. Consequently, excessive Zn^{2+} are effective in reducing the poling state and in depressing the domain switching of BCZT- x Zn ceramics; thus, they degrade the dielectric, ferroelectric and piezoelectric properties.

Mn as an interesting impurity exhibits multivalence states (Mn^{2+} , Mn^{3+} , and Mn^{4+}), and has been extensively used to substitute the A- and/or B-site ions of ferroelectrics for tailoring electrical properties [41]. Typically, it manifests itself as Mn^{2+} when sintering at high temperature above 850 °C. Meng et al. reported that the addition of 0.25 mol% MnO_2 promotes grain growth, improves the ferroelectricity of the ceramics and strengthens ferroelectric tetragonal-ferroelectric orthorhombic phase transition near 40 °C [42]. Such ceramics exhibit the optimum piezoelectric properties ($d_{33} = 306$ pC/N and $k_p = 42.2\%$, respectively). Excess MnO_2 inhibits the grain growth and degrades the ferroelectric and piezoelectric properties of the ceramics. Wu et al. reported similar results: the 0.15 wt% MnO doped BZT-BCT ceramics have optimum electrical properties: $d_{33} = 382$ pC/N, $k_p = 44.5\%$, $\epsilon_r = 2611$, and $\tan\delta = 0.63\%$. Besides, they also observed the double hysteresis loop when MnO dopant exceeds 0.3 wt%, which indicates the reversible domain switching dominating by the acceptor defect dipoles [43].

3.1.2. Donor Doping

A donor dopant has a higher oxidation number than that of the host cation. This will create cationic vacancies, either A-site or B-site vacancies in the perovskite structure. The donor dopant may effectively reduce the Curie temperature and facilitate the domain switching behavior, characterized as slim hysteresis loops with small coercive field and hysteresis loss.

Li et al. reported that, with the introduction of the donor Dy at A-site, the BZT-BCT ceramics possessed improved temperature stability. Besides the high piezoelectric coefficient of $d_{33} = 366$ pC/N and planar electromechanical coupling factor of $k_p = 43.0\%$, the Dy-doped BZT-BCT ceramics exhibited stable electromechanical coupling coefficients over a common usage temperature range of 20–100 °C [44]. They also revealed similar results in Ho-doped BZT-BCT ceramics [45].

As another common donor dopant to A-site, La^{3+} is often employed to enhance the electrical or mechanical responses under small AC field while reducing the loss in ferroelectric ceramics. Sun et al. reported that a small amount of La^{3+} (~0.15%) resulted in an increase of d_{33} at 50 °C due to the coexistence of orthorhombic and tetragonal phases. Besides, the 0.15 mol% La doped BZT-BCT ceramics turned to the semi-conductor and showed positive temperature coefficient (PTC) behavior [46]. Other donor dopants such as Cr^{3+} and Ga^{3+} also showed excellent improvements of d_{33} [47,48].

Besides the mono-element doped ceramics, compound doped BZT-BCT are also investigated. Wu et al. investigated the BiFeO_3 doped BZT-BCT ceramics [49]. Here, Bi^{3+} acted as the donor dopant at A-site while Fe^{3+} as the acceptor at B-site. By addition of BiFeO_3 , the grain size becomes smaller, and these ceramics become denser. The 0.2 mol% BiFeO_3 doped BZT-BCT ceramics demonstrated an improved piezoelectric behavior ($d_{33} \sim 405$ pC/N and $k_p \sim 0.44$). Tian et al. added Er^{3+} and La^{3+} into the BZT-BCT ceramics and found Er^{3+} first substituted A sites and then B sites in the matrix of ABO_3 structure. The elevated piezoelectric constant ($d_{33} \sim 200$ pC/N) and receded mechanical quality factor ($Q_m \sim 70$) at with 0.12% La^{3+} doping and 0.2% Er^{3+} doping showed “softening effect” by donor doping [50].

Extensive studies with other donor dopants were also carried on the BZT-BCT ceramics [30,51–54], as shown in Figure 2.

3.1.3. Equivalent Doping

Researchers have tried other doping with equivalent valence as the A-site or B-site to achieve MPB in the BaTiO_3 ceramics [55–60]. Zhou et al. designed a new Pb-free piezoelectric system $\text{Ba}(\text{Hf}_{0.2}\text{Ti}_{0.8})\text{O}_3\text{-(Ba}_{0.7}\text{Ca}_{0.3})\text{TiO}_3$, which yields high piezoelectricity with $d_{33} \sim 550$ pC/N, comparable to that of the best Pb-based material PZT-5H ($d_{33} \sim 590$ pC/N). Besides, their study suggests the non-isotropy of polarization at triple point by precise detection of transitional thermal hysteresis. Previously, the isotropy at triple point was always taken as the basic assumption in related modeling work and understanding [56]. Xue et al. designed a similar Pb-free pseudo-binary system, $\text{Ba}(\text{Sn}_{0.12}\text{Ti}_{0.88})\text{O}_3\text{-x}(\text{Ba}_{0.7}\text{Ca}_{0.3})\text{O}_3$, characterized by a phase boundary starting from a critical triple point of a paraelectric cubic phase, ferroelectric rhombohedral, and tetragonal phases [57]. The optimal composition BTS-30BCT exhibits a high piezoelectric coefficient $d_{33} = 530$ pC/N at room temperature.

For the equivalent doping of A-site, one of the most typical substitution is Sr^{2+} , which can contribute to the microstructure by increasing grain size and density, and at the same time decrease T_c [34,36,58,59]. As a result of fine microstructure and lower T_c , excellent piezoelectric properties with large d_{33} of 534 pC/N was exhibited in Bai and Li's work when 0.03 mol Sr^{2+} was doped [34]. Sn^{4+} is another commonly used element locating at B-site to enhance the piezoelectric properties of lead-free piezoelectric ceramics, especially in BT based ceramics [57,60]. In Ding and Liu's work, the co-doping of Sn^{4+} and Sr^{2+} could lead to good piezoelectrical properties of $d_{33} = 514$ pC/N and $k_p = 52.62\%$, although smaller grain size was obtained comparing with pure BZT-BCT ceramics, which is different from many other dopants that usually enhance the grain growth with low content [36].

3.2. Grain Size Effect and Sintering Aids

It is well known that grain size can have a significant influence on the properties of ferroelectric ceramics. For BZT-BCT based ceramics, the benefits to d_{33} from large grain size are extremely obvious, as shown in Figure 2. Elements acting as sintering aids such as Ce, Cu, Si, Li, etc. present brilliant performance. As the grain size decreased to the micron level, the permittivity at room temperature increased. The increase in permittivity can be understood in terms of the twinning behavior of polycrystals with decreasing grain size [61].

Hao et al. fabricated various BZT-50BCT ceramics with different grain size ranging from 0.4 to 32 μm . As grain size decreases, the diffuse phase transition behavior is enhanced. As the grains grow up to more than 10 μm , samples exhibit good piezoelectric properties with $k_p > 0.48$,

$k_t > 0.46$, $d_{33} > 470$ pC/N, and $d_{33}^* > 950$ pm/V. Besides, the increasing grain size effectively enhances the resistance to thermal depolarization [62].

In application, sintering aids are usually employed to enlarge the grain size and modify the microstructure to lower the sintering temperature and at the same time enhance the performance [28,29,37,63,64]. SiO₂, Li⁺, and CuO are widely used as the sintering aid of ceramics and exhibited good contributions in BZT-BCT system. In Chen's work, the dopant of Li⁺ reduced the sintering temperature of BZT-50BCT from 1540°C to 1400°C and piezoelectric performance with $d_{33} = 512$ pC/N and $k_p = 49\%$ were obtained [37]. In the work of co-doping of CeO₂ and Li₂CO₃, adding of Li₂CO₃ could largely decrease the sintering temperature from 1450°C to 1050°C comparing with the composition of CeO₂ dopant only [29]. Liu systematically studied the effect of SiO₂ dopant on the dielectric, ferroelectric and piezoelectric properties of the BZT-50BCT ceramics sintered at different temperatures and the results show that doping of SiO₂ could enhance P_r and d_{33} while reducing E_c . They obtained d_{33} of 500 pC/N [39,65]. CuO was also found to be effective on decreasing sintering temperature and modifying the microstructure of BZT-BCT ceramics, thus enhanced piezoelectric properties were achieved due to the large grain size caused by CuO [30,46,54]. The co-doping of CuO and B₂O₃ can largely benefit the morphology and enhance the piezoelectric properties [66]. Besides, some other substitution doping elements can also contribute to the sintering process at the same time such as Zn and Mn. In Wu's work, the grain size of ZnO doped BZT-BCT ceramic increased and surface morphologies became denser with the help of ZnO [35]. Similarly, MnO could also help sintering process greatly and benefit the piezoelectric performance [43,67].

4. For other Applications

It is well accepted that the easy polarization extension and rotation mechanism (low energy barriers for polarization variation) are the two most important intrinsic factors contributing to the enhanced physical properties [68,69]. Besides the good piezoelectric performance, BZT-BCT also exhibits other good properties due to its easy polarization rotation and easy domain wall motion.

4.1. Electrocaloric Effect

Electrocaloric effect (ECE) is a phenomenon that the change in adiabatic temperature and/or entropy of a dielectric material is induced by the application and removal of an electric field due to the change in the dipolar state of the material. In general, the ECE is parameterized by the adiabatic temperature change (ΔT), and the electrocaloric efficiency ($\Delta T/\Delta E$). The main technical challenge in lead-free ferroelectric bulk materials is to generate a giant electrocaloric temperature change ΔT under a relatively low electric field [70].

BZT-BCT has attracted much attention due to its relatively low coercive field and large polarization. Besides, the low Curie temperature also benefits the applications at room temperature. Sanjalp et al. reported that 0.65BZT-0.35BCT ceramics exhibited a ΔT of 0.33 °C and $\Delta T/\Delta E$ of 0.165 K mm kV⁻¹ at 65 °C under an electric field change $\Delta E = 20$ kV/cm [71]. G. Singha et al. reported large ECE in BZT-BCT ceramics [72]. They revealed that BZT-0.8BCT possessed an electro-caloric coefficient as high as 0.253 K mm/kV near tetragonal-to-cubic phase transition. They ascribed the high ECE to the higher polarization flexibility. Wang et al. performed direct measurements for BZT-BCT ceramics in non-adiabatic and non-equilibrium conditions. They found that BZT-0.7BCT showed the maximal ECE temperature change (ΔT_{ECE}) of 0.55 K was recorded for an applied field of 40 kV/cm at $T = 85$ °C [73]. Besides the good performance, they also revealed a very large discrepancy between the indirectly estimated and the directly measured ΔT_{ECE} . This was attributed to non-adiabatic conditions of the experiment resulting in a heat exchange with the environment.

4.2. Fluorescence

In recent years, ferroelectrics doped with rare earth elements have attracted great attention owing to their excellent multifunctional properties [74,75]. Multi-property coupling among the presence

of an electric field, mechanical stress and photons can introduce many applications as piezoelectric ceramics, mechano-luminescence and electro-luminescence materials. Peng Du et al. investigated the fluorescence intensity ratio of green up conversion emissions at 525 and 550 nm in the temperature range of 200–443 K for Er-doped BZT-BCT ceramics. The maximum sensing sensitivity and temperature resolution were found to be 0.0044 K^{-1} and 0.4 K, respectively, suggesting that Er-doped 0.5BZT-0.5BCT ferroelectric ceramic possesses potential application in optical temperature sensing [52,76].

Jiang Wu et al. reported that 0.5 mol% Er^{3+} BZT-BCT ceramics, synthesized via a sol-gel synthesis route and a ceramic sintering process, possessed excellent photoluminescence performance, which is sensitive to compositional changes [52]. The morphotropic phase boundary composition exhibited the maximum photoluminescence peak intensity at 550 nm.

4.3. Energy Storage

In theory, the energy density J corresponds to relative permittivity and dielectric breakdown strength (BDS) according to the definition $J = 1/2\varepsilon_0\varepsilon_r E_{\text{max}}^2$. For high energy storage density, ferroelectrics are expected to possess large saturated polarization, small remnant polarization and high BDS. BZT-BCT ceramics have evoked much interest. For certain compositions, this system exhibits large permittivity of 8400, triple that of pure BaTiO_3 ceramics. For the $\text{Ba}(\text{Ti}, \text{Zr})\text{O}_3$ -rich compositions, this system gradually transforms to the relaxor ferroelectrics, which exhibit diffusion phase transition with broadened permittivity peaks and slim ferroelectric hysteresis loops of large maximum polarization and small remnant polarization. These characteristics may favor the high energy density applications. Venkata et al. reported a significant increase in the permittivity with relatively low dielectric losses in the Zr-rich BZT-BCT ceramics [77]. $x\text{BZT-BCT}$ ($x = 0.10, 0.15, 0.20$) ceramics exhibited the electric breakdown strength as 134–170 kV/cm and high permittivity of 5200–8400. The consequent energy storage density can even reach 0.98 J/cm^3 . Besides the pure ceramics form, the addition of glass may effectively enhance the BDS and consequently promote energy storage density [77]. Liu et al. employed glass addition $\text{BaO-SrO-TiO}_2\text{-Al}_2\text{O}_3\text{-SiO}_2\text{-BaF}_2$ into BZT-0.15BCT ceramics, which exhibited a large permittivity of 3458 at 25 °C under 1 kHz, slim hysteresis loop with the maximum polarization of $12.53 \mu\text{C/cm}^2$ and a remnant polarization of $4.05 \mu\text{C/cm}^2$ [78]. Microstructural observation indicated that the average grain size reduced significantly with increasing the glass concentration. Macroscopically, the glass ceramics exhibited diffusion phase transition with reduced peak permittivity but broad peak with relatively large permittivity of around 1000 within the room temperature region. Meanwhile the electrical breakdown strength (BDS) of the glass modified ceramics was nearly quadruple to the pure ceramics form. Energy storage performance of the glass modified ceramics, both 419.4 kJ/m^3 calculated from the product of permittivity and square of BDS and 192.8 kJ/m^3 from the integration of the hysteresis loop under the electric field of 9.6 kV/mm, showed significant superiority to that of the pure ceramic form [78]. Besides, they explored the mechanism for the enhanced energy storage property by thermal stimulated current measurements, which may reveal both polarization and charge transport process [79].

5. Future prospects

5.1. Soft or Hard Modifications on BZT-BCT Ceramics

Ferroelectrics are rarely used in a chemically pure form and doping is always employed with the goal of tailoring the properties for specific applications. Most doping effects can be categorized into “hard” and “soft” effect. “Hard” effects are obtained by acceptor doping. The defect dipoles (acceptor-oxygen vacancy) can stabilize the domain structure (no matter the volume effect or the pinning effect) [80]. As macroscopic consequences, high coercive field, low permittivity and low dielectric losses are obtained. Donor dopants result in “soft” effect, i.e. high dielectric losses, low conductivity, low coercive field and high piezoelectric coefficients [81].

Further research should focus on revealing “soft” and “hard” effects within the MPB region of the present BZT-BCT ceramics. Further, the properties of BZT-BCT ceramics can be tailored to satisfy various applications and reveal the physics behind them.

5.2. BZT-BCT in other Forms—Single Crystal and Thin Film

It is common sense in the piezoelectric community that the single crystal always exhibits 3–4 times higher piezoelectric effect than that of a ceramic. Besides the better properties, single crystals can also be considered as standard materials to ascertain the structure properties. However, it is difficult to grow large scale single crystals with the perovskite structures. Thus far, several methods have been employed to generate good BZT-BCT single crystal samples and have not obtained satisfactory results to date [82].

Although intensive research up to date has been inclined to bulk materials, it is certainly obvious that the films will be the focus of the future industry. Since films exhibit small volume but large geometrical flexibility, can be easy for on-chip integration, which is a prerequisite for incorporation into microelectron devices. However, the development of films still lags behind bulk counterparts. For BZT-BCT films, several techniques have been employed, such as PLD, sputtering and CSD. Hereinto, the films fabricated via PLD method exhibited d_{33} of 60–140 pm/V depending on different orations [83,84]. The study of BZT-BCT film is still deficient. Further property enhancement and functionality enrichment are still the objectives to be pursued.

Author Contributions: Wenfeng Liu conceived and designed the manuscript, Lu Cheng wrote the manuscript, and Shengtao Li modified the manuscript.

Funding: This work was funded by the National Natural Science Foundation of China (51422704) and State Key Laboratory of Electrical Insulation and Power Equipment, Xi’an Jiaotong University (EIPE14113).

Conflicts of Interest: The authors declare no conflict of interest.

References

1. Bernard, J.; Hans, J. Piezoelectric Ceramics. *Mullard* **1974**, *15*, 193–211.
2. Damjanovic, A. Ferroelectric, dielectric and piezoelectric properties of ferroelectric thin films and ceramics. *Rep. Prog. Phys.* **1998**, *61*, 1267–1324. [[CrossRef](#)]
3. European Commission. EU-Directive 2011/65/EU: Restriction of the use of certain hazardous substances in electrical and electronic equipment (RoHS). *Off. J. Eur. Union* **2011**, *88*, L174.
4. European Commission. Directive 2002/96/EC: Waste electrical and electronic equipment (WEEE). *Off. J. Eur. Union* **2003**, *24*, L37.
5. Rodel, J.; Jo, W.; Seifert, K.T.P.; Anton, E.; Granzow, T.; Damjanovic, D. Perspective on the Development of Lead-free Piezoceramics. *J. Am. Ceram. Soc.* **2009**, *92*, 1153–1177. [[CrossRef](#)]
6. Rubio-Marcos, F.; Ochoa, P.; Fernandez, J. Sintering and properties of lead-free (K, Na, Li) (Nb, Ta, Sb)O₃ ceramics. *J. Eur. Ceram. Soc.* **2007**, *27*, 4125–4129. [[CrossRef](#)]
7. Murakami, S.; Wang, D.; Mostaed, A.; Khesro, A.; Feteira, A.; Sinclair, D.; Fan, Z. High strain (0.4%) Bi(Mg_{2/3}Nb_{1/3})O₃-BaTiO₃-BiFeO₃ lead-free piezoelectric ceramics and multilayers. *J. Am. Ceram. Soc.* **2018**, *101*, 5428–5442. [[CrossRef](#)]
8. Diez-Betriu, X.; Garcia, J.; Ostos, C.; Boya, A.; Ochoa, D.; Mestres, L. Phase transition characteristics and dielectric properties of rare-earth (La, Pr, Nd, Gd) doped Ba (Zr_{0.09}Ti_{0.91})O₃ ceramics. *Mater. Chem. Phys.* **2011**, *125*, 493–499. [[CrossRef](#)]
9. Liu, W.; Ren, X. Large non-linear piezoelectric effect due to recoverable domain switching. In Proceedings of the 2009 18th IEEE International Symposium on the Applications of Ferroelectrics, Xi’an, China, 23–27 August 2009.
10. Bao, H.; Zhou, C.; Xue, D.; Gao, J.; Ren, X. A modified lead-free piezoelectric BZT-xBCT system with higher TC. *J. Phys. D Appl. Phys.* **2010**, *43*, 465401. [[CrossRef](#)]

11. Su, S.; Zuo, R.; Lu, S.; Xu, Z.; Wang, X.; Li, L. Poling dependence and stability of piezoelectric properties of $\text{Ba}(\text{Zr}_{0.2}\text{Ti}_{0.8})\text{O}_3\text{-(Ba}_{0.7}\text{Ca}_{0.3})\text{TiO}_3$ ceramics with huge piezoelectric coefficients. *Curr. Appl. Phys.* **2011**, *11*, S120–S123. [[CrossRef](#)]
12. Yang, R.; Fu, W.; Deng, X.; Tan, Z.; Zhang, Y.; Han, L. Preparation and Characterization of $(\text{Ba}_{0.88}\text{Ca}_{0.12})(\text{Zr}_{0.12}\text{Ti}_{0.88})\text{O}_3$ Powders and Ceramics Produced by Sol-Gel Process. *Adv. Mater. Res.* **2010**, *148–149*, 1062–1066. [[CrossRef](#)]
13. Ehmke, M.C.; Glaum, J.; Hoffman, M.; Blendell, J.E. In Situ X-ray Diffraction of Biased Ferroelastic Switching in Tetragonal Lead-free $(1-x)\text{Ba}(\text{Zr}_{0.2}\text{Ti}_{0.8})\text{O}_3\text{-}x(\text{Ba}_{0.7}\text{Ca}_{0.3})\text{TiO}_3$ Piezoelectrics. *J. Am. Ceram. Soc.* **2013**, *96*, 2913–2920. [[CrossRef](#)]
14. Gao, X.R.J.; Zhang, L.; Xue, D.; Kimoto, T.; Song, M.; Zhong, L. Symmetry determination on Pb-free piezoceramic $0.5\text{Ba}(\text{Zr}_{0.2}\text{Ti}_{0.8})\text{O}_3\text{-}0.5(\text{Ba}_{0.7}\text{Ca}_{0.3})\text{TiO}_3$ using convergent beam electron diffraction method. *J. Appl. Phys.* **2014**, *115*, 054108. [[CrossRef](#)]
15. Keeble, D.S.; Benabdallah, F.; Thomas, P.; Maglione, M.; Kreisel, J. Revised structural phase diagram of $(\text{Ba}_{0.7}\text{Ca}_{0.3}\text{TiO}_3)\text{-(BaZr}_{0.2}\text{Ti}_{0.8}\text{O}_3)$. *Appl. Phys. Lett.* **2013**, *102*, 092903. [[CrossRef](#)]
16. Woodward, D.I.; Dittmer, R.; Jo, W.; Walker, D.; Keeble, D.S.; Dale, M.W.; Rodel, J. Investigation of the Depolarisation Transition in Bi-Based Relaxor Ferroelectrics. *J. Appl. Phys.* **2014**, *115*, 114109. [[CrossRef](#)]
17. Dwivedi, A.; Qu, W.; Randall, C.A.; Damjanovic, D. Preparation and Characterization of High-Temperature Ferroelectric $x\text{Bi}(\text{Mg}_{1/2}\text{Ti}_{1/2})\text{O}_3\text{-}y\text{Bi}(\text{Zn}_{1/2}\text{Ti}_{1/2})\text{O}_3\text{-}z\text{PbTiO}_3$ Perovskite Ternary Solid Solution. *J. Am. Ceram. Soc.* **2011**, *94*, 4371–4375. [[CrossRef](#)]
18. Rossetti, G.; Khachatryan, A.; Akcay, G.; Ni, Y. Ferroelectric Solid Solutions with Morphotropic Boundaries: Vanishing Polarization Anisotropy, Adaptive, Polar Glass, and Two-Phase States. *J. Appl. Phys.* **2008**, *103*, 114113–114115. [[CrossRef](#)]
19. Rossetti, G.A.; Khachatryan, A. Inherent nanoscale structural instabilities near morphotropic boundaries in ferroelectric solid solutions. *Appl. Phys. Lett.* **2007**, *91*, 072909. [[CrossRef](#)]
20. Acosta, M.; Novak, N.; Jo, W.; Rödel, J. Relationship between electromechanical properties and phase diagram in the $\text{Ba}(\text{Zr}_{0.2}\text{Ti}_{0.8})\text{O}_3\text{-}x(\text{Ba}_{0.7}\text{Ca}_{0.3})\text{TiO}_3$ lead-free piezoceramic. *Acta Mater.* **2014**, *80*, 48–55. [[CrossRef](#)]
21. Yang, T.; Ke, X.; Wang, Y. Mechanisms Responsible for the Large Piezoelectricity at the Tetragonal-Orthorhombic Phase Boundary of $(1-x)\text{BaZr}_{0.2}\text{Ti}_{0.8}\text{O}_3\text{-}x\text{Ba}_{0.7}\text{Ca}_{0.3}\text{TiO}_3$ System. *Sci. Rep.* **2016**, *6*, 33392. [[CrossRef](#)] [[PubMed](#)]
22. Wang, P.; Li, Y.; Lu, Y. Enhanced piezoelectric properties of $(\text{Ba}_{0.85}\text{Ca}_{0.15})(\text{Ti}_{0.9}\text{Zr}_{0.1})\text{O}_3$ lead-free ceramics by optimizing calcination and sintering temperature. *J. Eur. Ceram. Soc.* **2012**, *31*, 2005–2012. [[CrossRef](#)]
23. Liu, W.; Ren, X. Large piezoelectric effect in Pb-free ceramics. *Phys. Rev. Lett.* **2009**, *103*, 1–4. [[CrossRef](#)]
24. Tian, Y.; Wei, L.; Chao, X.; Liu, Z.; Yang, Z. Phase Transition Behavior and Large Piezoelectricity Near the Morphotropic Phase Boundary of Lead-Free $(\text{Ba}_{0.85}\text{Ca}_{0.15})(\text{Zr}_{0.1}\text{Ti}_{0.9})\text{O}_3$ Ceramics. *Am. Ceram. Soc.* **2013**, *96*, 496–502.
25. Xue, D.; Zhou, Y.; Bao, H.; Zhou, C.; Gao, J. Elastic, piezoelectric, and dielectric properties of $\text{Ba}(\text{Zr}_{0.2}\text{Ti}_{0.8})\text{O}_3\text{-}50(\text{Ba}_{0.7}\text{Ca}_{0.3})\text{TiO}_3$ Pb-free ceramic at the morphotropic phase boundary. *J. Appl. Phys.* **2011**, *109*, 054110. [[CrossRef](#)]
26. Shin, S.; Kim, J.; Koh, J. Piezoelectric properties of $(1-x)\text{BZT-xBCT}$ system for energy harvesting applications. *J. Eur. Ceram. Soc.* **2018**, *38*, 4395–4403. [[CrossRef](#)]
27. Zhao, Z.; Li, X.; Ji, H.; Dai, Y.; Li, T. Microstructure and electrical properties in Zn-doped $\text{Ba}_{0.85}\text{Ca}_{0.15}\text{Ti}_{0.9}\text{Zr}_{0.1}\text{O}_3$ piezoelectric ceramics. *J. Alloys Compd.* **2015**, *637*, 291–296. [[CrossRef](#)]
28. Cui, Y.; Liu, X.; Jiang, M.; Zhao, X.; Shan, X.; Li, W.; Yuan, C.; Zhou, C. Lead-free $(\text{Ba}_{0.85}\text{Ca}_{0.15})(\text{Ti}_{0.9}\text{Zr}_{0.1})\text{O}_3\text{-CeO}_2$ piezoelectric coefficient obtained by low-temperature sintering. *Ceram. Int.* **2012**, *38*, 4761–4764. [[CrossRef](#)]
29. Huang, X.; Xing, R.; Gao, C.; Chen, Z. Influence of CeO_2 doping amount on property of BCTZ lead-free piezoelectric ceramics sintered at low temperature. *J. Rare Earths* **2014**, *32*, 733–737. [[CrossRef](#)]
30. Wu, Y.; Liu, X.; Zhang, Q.; Jiang, M.; Liu, Y.; Liu, X. High piezoelectric coefficient of $\text{Ba}_{0.85}\text{Ca}_{0.15}\text{Ti}_{0.9}\text{Zr}_{0.1}\text{O}_3\text{Sr}(\text{Cu}_{1/3}\text{Ta}_{2/3})\text{O}_3$ ceramics. *J. Mater. Sci. Mater. Electron.* **2013**, *24*, 5199–5203. [[CrossRef](#)]
31. Chao, X.; Wang, J.; Wei, L.; Gou, R.; Yang, Z. Electrical properties and low temperature sintering of BiAlO_3 doped $(\text{Ba}_{0.85}\text{Ca}_{0.15})(\text{Zr}_{0.1}\text{Ti}_{0.9})\text{O}_3$ lead-free piezoelectric ceramics. *J. Mater. Sci.* **2015**, *26*, 7331–7340. [[CrossRef](#)]

32. Cui, Y.; Yuan, C.; Liu, X.; Zhao, X.; Shan, X. Lead-free $(\text{Ba}_{0.85}\text{Ca}_{0.15})(\text{Ti}_{0.9}\text{Zr}_{0.1})\text{O}_3\text{-Y}_2\text{O}_3$ ceramics with large piezoelectric coefficient obtained by low-temperature sintering. *J. Mater. Sci. Mater. Electron.* **2013**, *24*, 654–657. [[CrossRef](#)]
33. Ma, J.; Liu, X.; Jiang, M.; Yang, H.; Chen, G.; Liu, X.; Qin, L.; Luo, C. Dielectric, ferroelectric, and piezoelectric properties of Sb_2O_3 -modified $(\text{Ba}_{0.85}\text{Ca}_{0.15})(\text{Zr}_{0.1}\text{Ti}_{0.9})\text{O}_3$ lead-free. *J. Mater. Sci. Mater. Electron.* **2014**, *25*, 992–996. [[CrossRef](#)]
34. Bai, W.F.; Li, W.; Shen, B.; Zhai, J.W. Piezoelectric and Strain Properties of Strontium-Doped BZT-BCT Lead-Free Ceramics. *High Perform. Ceram.* **2012**, *512–515*, 1385–1389. [[CrossRef](#)]
35. Wu, J.; Xiao, D.; Wu, W.; Chen, Q.; Zhu, J.; Yang, Z.; Wang, J. Role of room-temperature phase transition in the electrical properties of $(\text{Ba,Ca})(\text{Ti,Zr})\text{O}_3$ ceramics. *Scr. Mater.* **2011**, *65*, 771–774. [[CrossRef](#)]
36. Liu, X.; Chen, Z.; Fang, B.; Ding, J.; Zhao, X.; Xu, H.; Luo, H. Enhancing piezoelectric properties of BCZT ceramics by Sr and Sn co-doping. *J. Alloys Compd.* **2015**, *640*, 128–133. [[CrossRef](#)]
37. Chen, X.; Ruan, X.; Zhao, K.; He, X.; Zeng, J.; Li, Y.; Zheng, L.; Park, C.H.; Li, G. Low sintering temperature and high piezoelectric properties of Li-doped $(\text{Ba,Ca})(\text{Ti,Zr})\text{O}_3$ lead-free ceramics. *J. Alloys Compd.* **2015**, *632*, 103–109. [[CrossRef](#)]
38. Cui, Y.; Liu, X.; Jiang, M.; Wang, Y.H.; Su, Q.; Wang, H. Lead-free $(\text{Ba}_{0.7}\text{Ca}_{0.3})\text{TiO}_3\text{-Ba}(\text{Zr}_{0.2}\text{Ti}_{0.8})\text{O}_3\text{-xwt}\%\text{CuO}$ ceramics with high piezoelectric coefficient by low-temperature sintering. *J. Mater. Sci.* **2012**, *23*, 1342–1345. [[CrossRef](#)]
39. Liu, W.; Li, S. Effect of SiO_2 doping on the dielectric, ferroelectric and piezoelectric properties of $(\text{Ba}_{0.7}\text{Ca}_{0.3})(\text{Zr}_{0.2}\text{Ti}_{0.8})\text{O}_3$ ceramics with different sintering temperatures. *IEEE Trans. Dielectr. Electr. Insul.* **2015**, *22*, 734–738. [[CrossRef](#)]
40. Parjansri, P.; Pengpat, K.; Rujijanagul, G.; Tunkasiri, T.; Intatha, U.; Eitssayeam, S. Effect of Zn^{2+} and Nb^{5+} Co-Doping on Electrical Properties of BCZT Ceramics by the Seed-Induced Method. *Ferroelectrics* **2014**, *458*, 91–97. [[CrossRef](#)]
41. Xu, C.; Yao, Z.; Lu, K.; Hao, H.; Yu, Z.; Cao, M.; Liu, H. Enhanced piezoelectric properties and thermal stability in tetragonal-structured $(\text{Ba,Ca})(\text{Zr,Ti})\text{O}_3$ piezoelectrics substituted with trace amount of Mn. *Ceram. Int.* **2016**, *42*, 16109–16115. [[CrossRef](#)]
42. Jiang, M.; Lin, Q.; Lin, D.; Zheng, Q.; Fan, X.; Wu, X.; Sun, H.; Wan, Y.; Wu, L. Effects of MnO_2 and sintering temperature on microstructure, ferroelectric, and piezoelectric properties. *J. Mater. Sci.* **2013**, *48*, 1035–1041. [[CrossRef](#)]
43. Wu, J.; Wang, Z.; Zhang, B.; Zhu, J.; Xiao, D. $\text{Ba}_{0.85}\text{Ca}_{0.15}\text{Ti}_{0.90}\text{Zr}_{0.10}\text{O}_3$ Lead-free Ceramics with a Sintering Aid of MnO. *Integr. Ferroelectr.* **2013**, *141*, 89–98. [[CrossRef](#)]
44. Li, W.; Xu, Z.; Chu, R.; Fu, P.; Zang, G. Temperature Stability in Dy-Doped $(\text{Ba}_{0.99}\text{Ca}_{0.01})(\text{Ti}_{0.98}\text{Zr}_{0.02})\text{O}_3$ Lead-Free Ceramics with High Piezoelectric Coefficient. *J. Am. Ceram. Soc.* **2011**, *94*, 3181–3183. [[CrossRef](#)]
45. Li, W.; Xu, Z.; Chu, R.; Fu, P.; An, P. Effect of Ho doping on piezoelectric properties of BCZT ceramics. *Ceram. Int.* **2012**, *38*, 4353–4355. [[CrossRef](#)]
46. Sun, Z.; Pu, Y.; Dong, Z.; Hu, Y.; Liu, X.; Wang, P.; Ge, M. Dielectric and piezoelectric properties and PTC behavior of $\text{Ba}_{0.9}\text{Ca}_{0.1}\text{Ti}_{0.9}\text{Zr}_{0.1}\text{O}_3\text{-xLa}$ ceramics prepared by hydrothermal method. *Mater. Lett.* **2014**, *118*, 1–4. [[CrossRef](#)]
47. Xia, X.; Jiang, X.; Chen, C.; Jiang, X.; Tu, N.; Chen, Y. Effects of Cr_2O_3 doping on the microstructure and electrical properties of $(\text{Ba,Ca})(\text{Zr,Ti})\text{O}_3$ lead-free ceramics. *Front. Mater. Sci.* **2016**, *10*, 203–210. [[CrossRef](#)]
48. Ma, J.; Liu, X.; Li, W. High piezoelectric coefficient and temperature stability of Ga_2O_3 -doped. *J. Alloys Compd.* **2013**, *581*, 642–645. [[CrossRef](#)]
49. Wu, J.; Wu, W.; Xiao, D.; Wang, J.; Yang, Z.; Peng, Z.; Chen, Q.; Zhu, J. $(\text{Ba,Ca})(\text{Ti,Zr})\text{O}_3\text{-BiFeO}_3$ lead-free piezoelectric ceramics. *Curr. Appl. Phys.* **2012**, *12*, 534–538. [[CrossRef](#)]
50. Tian, Y.; Li, S.; Gong, Y.; Meng, D.; Wang, J.; Jing, Q. Effects of Er^{3+} -doping on dielectric and piezoelectric properties of $0.5\text{Ba}_{0.9}\text{Ca}_{0.1}\text{TiO}_3\text{-0.5BaTi}_{0.88}\text{Zr}_{0.12}\text{O}_3\text{-0.12}\%\text{La-xEr}$ lead-free ceramics. *J. Alloys Compd.* **2017**, *692*, 797–804. [[CrossRef](#)]
51. Parjansri, P.; Intatha, U.; Eitssayeam, S. Dielectric, ferroelectric and piezoelectric properties of Nb^{5+} doped BCZT ceramics. *Mater. Res. Bull.* **2015**, *65*, 61–67. [[CrossRef](#)]
52. Dai, J.; Du, P.; Xu, J.; Xu, C.; Luo, L. Piezoelectric and upconversion emission properties of Er^{3+} -doped $0.5\text{Ba}(\text{Zr}_{0.2}\text{Ti}_{0.8})\text{O}_3\text{-0.5}(\text{Ba}_{0.7}\text{Ca}_{0.3})\text{TiO}_3$ ceramic. *J. Rare Earths* **2015**, *33*, 391–396. [[CrossRef](#)]

53. Han, C.; Wu, J.; Pu, C.; Qiao, S.; Wu, B.; Zhu, J.; Xiao, D. High piezoelectric coefficient of Pr₂O₃-doped Ba_{0.85}Ca_{0.15}Ti_{0.90}Zr_{0.10}O₃ ceramics. *Ceram. Int.* **2012**, *38*, 6359–6363. [[CrossRef](#)]
54. Li, Q.; Ma, W.; Ma, J.; Meng, X.; Niu, B. High piezoelectric properties of Sm₂O₃ doped Ba_{0.85}Ca_{0.15}Ti_{0.90}Zr_{0.10}O₃ ceramics. *Mater. Technol.* **2016**, *31*, 18–23. [[CrossRef](#)]
55. Tian, Y.; Gong, Y.; Meng, D.; Cao, S. Structure and electrical properties of Ir⁴⁺-doped 0.5Ba_{0.9}Ca_{0.1}TiO₃-0.5BaTi_{0.88}Zr_{0.12}O₃-0.12%La ceramics via a modified Pechini method. *Mater. Lett.* **2015**, *153*, 44–46. [[CrossRef](#)]
56. Zhou, C.; Liu, W.; Xue, D.; Ren, X.; Bao, H. Triple-point-type morphotropic phase boundary based large piezoelectric Pb-free material—Ba(Ti_{0.8}Hf_{0.2})O₃-(Ba_{0.7}Ca_{0.3})TiO₃. *Appl. Phys. Lett.* **2012**, *100*, 222910. [[CrossRef](#)]
57. Xue, D.; Zhou, Y.; Bao, H.; Gao, J.; Zhou, C.; Ren, X. Large piezoelectric effect in Pb-free Ba(Ti,Sn)O₃-x(Ba,Ca)TiO₃ ceramics. *Appl. Phys. Lett.* **2011**, *99*, 3–6. [[CrossRef](#)]
58. Parjansri, P.; Intatha, U.; Eitssayeam, S.; Pengpat, K.; Rujijanagul, G.; Tunkasiri, T. Effects of Mn and Sr Doping on the Electrical Properties of Lead-Free 0.92BCZT-0.08BZT Ceramics. *Integr. Ferroelectr.* **2012**, *139*, 75–82. [[CrossRef](#)]
59. Liu, C.; Liu, X.; Wang, D.; Chen, Z.; Fang, B.; Ding, J. High piezoelectric coefficient of Ba^{0.85}Ca_{0.15}Ti_{0.9}Zr_{0.1}O₃-Sr(Cu_{1/3}Ta_{2/3})O₃ ceramics. *J. Mater. Sci. Mater. Electron.* **2014**, *40*, 9881–9887.
60. Kalyani, A.K.; Krishnan, H.; Sen, A.; Senyshyn, A.; Ranjan, R. Polarization switching and high piezoelectric response in Sn-modified BaTiO₃. *Phys. Rev. B Condens. Matter Mater. Phys.* **2015**, *91*, 1–13. [[CrossRef](#)]
61. Frey, M.H.; Payne, D.A. Grain-Size Effect on Structure and Phase Transformation for Barium Titanate. *Phys. Rev. B* **1996**, *54*, 3158–3167. [[CrossRef](#)]
62. Hao, J.; Bai, W.; Li, W.; Zhai, J. Correlation Between the Microstructure and Electrical Properties in High-Performance (Ba_{0.85}Ca_{0.15})(Zr_{0.1}Ti_{0.9})O₃ Lead-Free Piezoelectric Ceramics. *J. Am. Ceram. Soc.* **2012**, *95*, 1998–2006. [[CrossRef](#)]
63. Brajesh, K.; Kalyani, A.; Ranjan, R. Ferroelectric instabilities and enhanced piezoelectric response in Ce modified BaTiO₃ lead-free ceramics. *Appl. Phys. Lett.* **2015**, *106*, 12907. [[CrossRef](#)]
64. Ang, C.; Yu, Z.; Jing, Z.; Guo, R.; Bhalla, A.; Cross, L. Piezoelectric and electrostrictive strain behavior of Ce-doped BaTiO₃ ceramics. *Appl. Phys. Lett.* **2002**, *80*, 3424–3426. [[CrossRef](#)]
65. Liu, W.; Zhao, D.; Li, S. Doping effect of SiO₂/CeO₂ on the dielectric, ferroelectric and piezoelectric properties of (Ba_{0.7}Ca_{0.3})(Zr_{0.2}Ti_{0.8})O₃ ceramics. *Ferroelectrics* **2014**, *496*, 23–35.
66. Shin, S.-H.; Han, J.-D.; Yoo, J. Piezoelectric and dielectric properties of B₂O₃-added (Ba_{0.85}Ca_{0.15})(Ti_{0.915}Zr_{0.085})O₃ ceramics sintered at low temperature. *Mater. Lett.* **2015**, *154*, 120–123. [[CrossRef](#)]
67. Rubiomarcos, F.; Marchet, P.; Vendrell, X.; Romero, J.J.; Remondiere, F.; Mestres, L.; Fernandez, J.F. Effect of MnO doping on the structure, microstructure and electrical properties of the (K,Na,Li)(Nb,Ta,Sb)O₃ lead-free piezoceramics. *J. Alloys Compd.* **2011**, *509*, 8804–8811. [[CrossRef](#)]
68. Damjanovic, D. A morphotropic phase boundary system based on polarization rotation and polarization extension. *Appl. Phys. Lett.* **2010**, *97*, 062906. [[CrossRef](#)]
69. Fu, H.; Cohen, R.E. Polarization rotation mechanism for ultrahigh electromechanical response in single-crystal piezoelectrics. *Nature* **2000**, *403*, 281–283. [[CrossRef](#)] [[PubMed](#)]
70. Qian, X.S.; Ye, H.J.; Zhang, Y.T.; Gu, H.; Li, X.; Randall, C.; Zhang, Q. Giant electrocaloric response over a broad temperature range in modified BaTiO₃ ceramics. *Adv. Funct. Mater.* **2014**, *24*, 1300–1305. [[CrossRef](#)]
71. Sanliarp, M.; Shvartsman, V.V.; Acosta, M.; Dkhil, B.; Lupascu, D.C. Strong electrocaloric effect in lead-free 0.65Ba(Zr_{0.2}Ti_{0.8})O₃-0.35(Ba_{0.7}Ca_{0.3})TiO₃ ceramics obtained by direct measurements. *Appl. Phys. Lett.* **2015**, *106*, 062901. [[CrossRef](#)]
72. Singha, G.; Tiwari, V.S.; Gupta, P.K. Electro-caloric effect in (Ba_{1-x}Ca_x)(Zr_{0.05}Ti_{0.95})O₃: A lead-free ferroelectric material. *Appl. Phys. Lett.* **2013**, *103*, 202903. [[CrossRef](#)]
73. Wang, J.; Yang, T.; Chen, S.; Li, G.; Zhang, Q. Nonadiabatic direct measurement electrocaloric effect in lead-free Ba,Ca(Zr,Ti)O₃ ceramics. *J. Alloy Compd.* **2013**, *550*, 561–563. [[CrossRef](#)]
74. Wang, X.; Xu, C.N.; Yamada, H.; Nishikubo, K.; Zheng, X.G. Electro-mechano-optical conversions in Pr³⁺-doped BaTiO₃-CaTiO₃ ceramics. *Adv. Mater.* **2005**, *17*, 1254–1258. [[CrossRef](#)]
75. Zou, H.; Peng, D.; Wu, G.; Wang, X.; Bao, D.; Li, J.; Li, Y.; Yao, X. Polarization-induced enhancement of photoluminescence in Pr³⁺ doped ferroelectric diphase BaTiO₃-CaTiO₃ ceramics. *J. Appl. Phys.* **2013**, *114*, 5–10. [[CrossRef](#)]

76. Ba, Z.O. Optical temperature sensor based on upconversion emission in Er-doped ferroelectric $0.5\text{Ba}(\text{Zr}_{0.2}\text{Ti}_{0.8})\text{O}_3\text{-}0.5(\text{Ba}_{0.7}\text{Ca}_{0.3})\text{TiO}_3$ ceramic. *J. Appl. Phys.* **2014**, *5*, 2–6.
77. Puli, V.S.; Pradhan, D.K.; Chrisey, D.B.; Tomozawa, M.; Sharma, G.L.; Scott, J.F.; Katiyar, R.S. Structure, dielectric, ferroelectric, and energy density properties of (1-x) BZT-xBCT ceramic capacitors for energy storage applications. *J. Mater. Sci.* **2013**, *48*, 2151–2157. [[CrossRef](#)]
78. Liu, W.; Ping, W.; Li, S. Enhanced energy storage properties of $\text{Ba}(\text{Zr}_{0.2}\text{Ti}_{0.8})\text{O}_3\text{-}0.15(\text{Ba}_{0.7}\text{Ca}_{0.3})\text{TiO}_3$ ceramics with BaO-SrO-TiO₂-Al₂O₃-SiO₂-BaF₂ glass addition. *Energy Technol.* **2016**, *5*, 1423–1428. [[CrossRef](#)]
79. Liu, W.; Ping, W.; Li, S. Enhanced energy storage property in glass-added $\text{Ba}(\text{Zr}_{0.2}\text{Ti}_{0.8})\text{O}_3\text{-}0.15(\text{Ba}_{0.7}\text{Ca}_{0.3})\text{TiO}_3$ ceramics and the charge relaxation. *Ceram. Int.* Accepted.
80. Vendrell, X.; García, J.; Bril, X.; Ochoa, D.; Mestres, L.; Dezanneau, G. Improving the functional properties of $(\text{K}_{0.5}\text{Na}_{0.5})\text{NbO}_3$ piezoceramics by acceptor doping. *J. Eur. Ceram. Soc.* **2015**, *35*, 125–130. [[CrossRef](#)]
81. Liu, W.; Chen, W.; Yang, L.; Zhang, L.; Wang, Y.; Zhou, C.; Li, S.; Ren, X. Ferroelectric aging effect in hybrid-doped BaTiO₃ ceramics and the associated large recoverable electrostrain. *Appl. Phys. Lett.* **2006**, *89*, 1–4. [[CrossRef](#)]
82. Palneedi, H.; Annapureddy, V.; Lee, H.; Choi, J.; Choi, S.; Chung, S.; Kangad, S.-J.L.; Ryu, J. Strong and anisotropic magnetoelectricity in composites of magnetostrictive Ni and solid-state grown lead-free piezoelectric BZT-BCT single crystals. *J. Asian Ceram. Soc.* **2017**, *5*, 36–41. [[CrossRef](#)]
83. Xu, J.B.; Shen, B.; Zhai, J.W. Dielectric, ferroelectric and optical properties of $\text{BaZr}_{0.2}\text{Ti}_{0.8}\text{O}_3$ thin films prepared by sol-gel-hydrothermal process. *J. Sol. Gel Sci. Technol.* **2010**, *55*, 343–347. [[CrossRef](#)]
84. Luo, B.; Wang, D.; Duan, M.; Li, S. Orientation-Dependent Piezoelectric Properties in Lead-Free Epitaxial $0.5\text{BaZr}_{0.2}\text{Ti}_{0.8}\text{O}_3\text{-}0.5\text{Ba}_{0.7}\text{Ca}_{0.3}\text{TiO}_3$ Thin Films. *Appl. Phys. Lett.* **2013**, *103*, 385–391. [[CrossRef](#)]



© 2019 by the authors. Licensee MDPI, Basel, Switzerland. This article is an open access article distributed under the terms and conditions of the Creative Commons Attribution (CC BY) license (<http://creativecommons.org/licenses/by/4.0/>).